Computational Biology and Chemistry 92 (2021) 107490

Contents lists available at ScienceDirect

Computational Biology and Chemistry

journal homepage: www.elsevier.com/locate/cbac

Research Article

In silico and *in vitro* assessment of androgen receptor antagonists

Onur Serçinoğlu [a], Ceyhun Bereketoglu [b], Per-Erik Olsson [c], Ajay Pradhan [c,*]

[a] Department of Bioengineering, Faculty of Engineering, Gebze Technical University, 41400, Gebze, Kocaeli, Turkey
[b] Iskenderun Technical University, Faculty of Engineering and Natural Sciences, Department of Biomedical Engineering, Hatay, Turkey
[c] Biology, The Life Science Center, School of Science and Technology, Örebro University, SE-701 82, Örebro, Sweden

ARTICLE INFO

Keywords:
Helix 12
Antiandrogen
Prostate
Endocrine disruption
Pollutants

ABSTRACT

There is a growing concern for male reproductive health as studies suggest that there is a sharp increase in prostate cancer and other fertility related problems. Apart from lifestyle, pollutants are also known to negatively affect the reproductive system. In addition to many other compounds that have been shown to alter androgen signaling, several environmental pollutants are known to disrupt androgen signaling *via* binding to androgen receptor (AR) or indirectly affecting the androgen synthesis. We analyzed here the molecular mechanism of the interaction between the human AR Ligand Binding Domain (hAR-LBD) and two environmental pollutants, linuron (a herbicide) and procymidone (a pesticide), and compared with the steroid agonist dihydrotestosterone (DHT) and well-known hAR antagonists bicalutamide and enzalutamide. Using molecular docking and dynamics simulations, we showed that the co-activator interaction site of the hAR-LBD is disrupted in different ways by different ligands. Binding free energies of the ligands were also ordered in increasing order as follows: linuron, procymidone, DHT, bicalutamide, and enzalutamide. These data were confirmed by *in vitro* assays. Reporter assay with MDA-kb2 cells showed that linuron, procymidone, bicalutamide and enzalutamide can inhibit androgen mediated activation of luciferase activity. Gene expression analysis further showed that these compounds can inhibit the expression of *prostate specific antigen* (*PSA*) and *microseminoprotein beta* (*MSMB*) in prostate cell line LNCaP. Comparative analysis showed that procymidone is more potent than linuron in inhibiting AR activity. Furthermore, procymidone at 10 μM dose showed equivalent and higher activity to AR inhibitor enzalutamide and bicalutamide respectively.

1. Introduction

Androgens are the key regulators of male sexual differentiation, such as proper growth, development and prostate function (Kortenkamp and Faust, 2010; Marker et al., 2003; Wang et al., 2007). Suppression of androgen functions either through inhibition of androgen synthesis or by antagonism of androgen receptor (AR) may result in serious health problems (Kortenkamp and Faust, 2010). The decline in sperm number and viability, hypospadias, cryptorchidism as well as testicular cancer are the common problems observed following AR modulation (Earl Gray et al., 2006; Foster, 2006; Wilson et al., 2008). There is an apparent increase in male reproductive health problems (Wilson et al., 2008) and consequently, concerns have been raised on environmental pollutants that can disrupt the androgen activity. It has been indicated that around 8% of all known chemicals show anti-androgenic activity and several chemicals including plasticizers, flame retardants and pesticides have been determined as anti-androgens (Kharlyngdoh et al., 2015; Kortenkamp and Faust, 2010; Vinggaard et al., 2008). Most of these chemicals are widely used in different products and as a result, they are released and accumulate into the environment. Hence, determining molecular mechanisms underlying the modes of action of such chemicals could be helpful to regulate their use and take preventive actions against their adverse effects.

The human AR (hAR) consists of three structural domains: a N-terminal transcriptional regulation domain, a DNA-binding domain (DBD), and a ligand Binding Domain (LBD) (Davey and Grossmann, 2016). The LBD is the region of hAR that is involved in ligand binding and includes well-characterized binding sites where an agonist or antagonist may bind and alter AR functions. The LBD consists of ligand binding pocket (LBP), C-terminal activation function 2 (AF2) site, and the binding function 3 (BF3) site (Davey and Grossmann, 2016; Tan et al., 2015). Androgens perform their function on hAR by binding to the LBP and thereby inducing subsequent structural rearrangements in the LBD that allow interaction with the co-activators *via* the AF2 site. On the other

* Corresponding author.
E-mail address: ajay.pradhan@oru.se (A. Pradhan).

https://doi.org/10.1016/j.compbiolchem.2021.107490
Received 23 October 2020; Received in revised form 20 April 2021; Accepted 20 April 2021
Available online 23 April 2021

hand, antagonists including environmental pollutants may exert their effect in different ways. First, an antagonist may compete with an agonist in binding to the LBP. In this case, the effect on the AF2 occurs in a way to prevent co-activator binding. Alternatively, an antagonist may directly bind to the AF2 site, and inhibit co-activator interaction. Finally, an antagonist may also bind to the BF3 site, and induce an allosteric effect propagating through the structure to the AF2 site (Tan et al., 2015).

Linuron is a phenyl-urea herbicide that is commonly used to suppress a number of broadleaf and grass weeds in various crops including soybean, cotton, corn, wheat, sugar cane, and potato, as well as many other fruits and vegetables (Bai et al., 2017; Spirhanzlova et al., 2017). It shows its herbicidal activity through inhibition of photosynthesis by targeting photosystem II reaction center and blocking electron transport that leads to the generation of oxidants (Jurado et al., 2011; Quintaneiro et al., 2017; Uren Webster et al., 2015). Concentrations up to 1.05 μg/L in a Canadian river (Woudneh et al., 2009) and 4.42 μg/L in a Florida stream (Schuler and Rand, 2008) have been detected in surface waters receiving agricultural runoff. In addition, linuron has been detected in drinking water and food residues (EPA, U., 2015; Spirhanzlova et al., 2017). Several studies have demonstrated that linuron may have an anti-androgenic activity. It has been shown that linuron competitively inhibits the binding of androgen to the AR *in vitro* (Freyberger et al., 2010; Kojima et al., 2004; Lambright et al., 2000; Orton et al., 2009; Wilson et al., 2007). Other studies have shown the anti-androgenic activity of linuron *in vivo* (Freyberger and Schladt, 2009; Kang et al., 2004; Lambright et al., 2000). In addition, linuron has adverse effects on the reproductive health of male rats, as it has been shown to reduce fetal testosterone levels *in vitro* and *in vivo*, and alter sexual differentiation *in utero* (Hotchkiss et al., 2004; Wilson et al., 2009).

Procymidone is an amide-type fungicide with both protective and curative properties used to control plant diseases such as gray mold on top of fruits, grapes and vegetables, and Sclerotinia rot of beans, vegetable crops and stone fruit (Hosokawa et al., 1993; Tomigahara et al., 2014; Wu et al., 2018). Procymidone is persistent in soil for several weeks since it is stable to light and temperature as well as moisture (Wu et al., 2018). Reported concentrations of procymidone ranged between 0.02 and 0.41 μg/L in drained water samples from a cherry orchard in the Mt. Lofty Ranges, South Australia, and 0.05 and 9.06 μg/L in a river near an agricultural region in South Africa (Dabrowski et al., 2002; Oliver et al., 2012). Moreover, procymidone has been detected with a concentration of 3.9 μg/L in water from the Jiulong River, China (Zheng et al., 2016). Some *in vitro* and *in vivo* studies have showed an AR antagonist activity of procymidone (Hosokawa et al., 1993; Kang et al., 2004; Nellemann et al., 2003; Vinggaard et al., 1999). Procymidone has also been demonstrated to have anti-androgenic activity *in vitro* and to alter reproductive development in male offspring (Ostby et al., 1999). However, in another study, procymidone was shown to have weak anti-androgenic activity in HeLa cells transiently transfected with an AREx3-luciferase reporter and full-length human or rat AR expression vectors (Tomigahara et al., 2014). In addition, an estrogenic activity of procymidone has also been demonstrated *in vitro* (Radice et al., 2006, 2004).

Although both *in vivo* and *in vitro* assays have indicated that linuron and procymidone have anti-androgenic activity, the underlying molecular mechanisms behind this antagonism is still unclear. Understanding how a ligand/compound binds to its macromolecular counterpart in full atomic detail could help to predict their mode of action and molecular mechanisms of toxicity. Recently, *in silico* approaches, particularly molecular docking and molecular dynamics simulations have emerged as key techniques in understanding and deciphering macromolecular structure-to-function relationships (Hollingsworth and Dror, 2018; Hospital et al., 2015). Furthermore, *in silico* approaches prior *in vitro* and/or *in vivo* analysis may reduce cost and animal use in scientific experimentations (Freires et al., 2017; Galli et al., 2014). In a previous study, the affinity of procymidone has been computed following a computational approach based on molecular modeling and docking. It has been suggested that the applied approach could be useful as a first step of chemical safety assessment and further *in vitro* and/or *in vivo* tests should be carried out (Galli et al., 2014). In the current study, we determined the antagonistic activities of linuron and procymidone with respect to dihydrotestosterone (DHT; a steroid hAR agonist) and well-characterized hAR antagonists bicalutamide and enzalutamide using both *in silico* and *in vitro* experimental methods. We first employed molecular docking to probe the interaction mechanism between the compounds and human AR Ligand Binding Domain (hAR-LBD). We then conducted molecular dynamics (MD) simulations to assess structural changes induced by antagonist or agonist binding to the hAR-LBD. Then, we determined the anti-androgenic activity of the compounds using reporter assay and gene expression study.

2. Materials and methods

2.1. Chemical

Procymidone (purity ≥98 %), linuron (purity ≥98 %), enzalutamide (purity ≥98 %), bicalutamide (purity ≥98 %) and dihydrotestosterone (DHT) (Supplementary Fig. 1) were purchased from Sigma and dissolved in dimethylsulfoxide (DMSO).

2.2. Molecular docking and dynamics simulations

Molecular (re-)docking simulations were conducted using LeDock (Liu and Xu, 2021), Autodock Vina (Trott and Olson, 2010), and GalaxyDock 3 (Yang et al., 2019). For Autodock Vina and LeDock, the size of the docking area ranged between 15 and 30 Å, depending on the size of each ligand. An exhaustiveness value of 25 was used for Autodock Vina simulations. A total of 20 and 50 binding poses were generated for each ligand by Autodock and LeDock, respectively. For GalaxyDock 3 simulations, docking grids with *grid_n_elem* of 61 in each direction and *grid_width* of 0.375 was used with appropriately defined center coordinates for each ligand binding site.

Molecular dynamics simulations were performed using gromacs version 2018.1 with GROMOS54A7 force-field. Since the force-fields used for biomolecular simulation in general does not include parameters for small molecules, parametrization of ligands was necessary. For this purpose, Automated Topology Builder (ATB) server (Malde et al., 2011) was used, which generates ligand parameters compatible with the used force-field using a pre-defined QM/MM calculation workflow. For each simulation, the system was first minimized for a maximum of 50,000 steps until the maximum force reached a level lower than 10 kJ/mol. Here, cutoff values of 1.2, 1.4 and 1.4 nm were used for neighbor lists, and as Coulomb and van-der Waals interactions, respectively. Particle Mesh Ewald (PME) method was used for treatment of long-range electrostatic interactions. Following energy minimization, the systems were subjected to NVT and NPT equilibration for 50,000 steps each at 310 K using the same cutoff values and settings as in minimization. Finally, NPT simulations were conducted for 500 ns as production simulations (for bicalutamide-hAR-LBD, the simulation lasted for 750 ns), and these were used in all analyses.

2.3. Analysis of MD simulations

Root Mean Square Distance (RMSD) and Fluctuation (RMSF) calculations were performed using biotite (Kunzmann and Hamacher, 2018) and ProDy (Bakan et al., 2011) based on alpha carbon coordinates from each simulation trajectory. To analyze how the ligands contacted the hAR-LBD throughout simulations, gRINN (Sercinoglu and Ozbek, 2018), was used to compute average non-bonded interaction energies between ligands and individual amino acids of hAR-LBD in simulation trajectories. The source code of gRINN was modified to support small molecules. Binding free energies of ligands were computed using

PRODIGY-LIG on 1500 snapshots from equilibrated portions of simulation trajectories (Kurkcuoglu et al., 2018).

2.4. Cell culture and exposure

MDA-kb2 cells (ATCC) were cultured in Leibovitz's L15 medium (Invitrogen) supplemented with 10 % fetal bovine serum (FBS, Hyclone), and antibiotic and antimycotic solution (Hyclone). Cells were maintained in a humidified incubator at 37 ºC. LNCaP cells (ATCC) were cultured in RPMI media (Invitrogen) supplemented with 10 % FBS and antibiotic and antimycotic solution. Cells were incubated in a humidified incubator at 37 ºC and 5 % CO2. For exposure, cells were trypsinized and the cells were counted and plated. MDAkb2 cells were plated on 24 well plates (Sarstedt) at 1 × 10e5 cells per well and 500 µL media. LNCaP cells were plated on 12 well plates at 1 × 10e5 cells per well and 1 mL media. Cells were incubated for 16−18 hours prior to exposure. For exposure, procymidone, linuron and DHT were prepared in respective media for the two cell lines and the exposure media was added with a volume of 1 mL for each well. Cells were exposed for 24 h at 37 ºC. The final DMSO was 0.01 % in control and treated cells. All the treatment and control samples were analyzed in quadruplicate.

2.5. Luciferase assay

Following exposure, MDA-kb2 cells were washed with phosphate buffered saline (PBS) and cells were then lysed with lysis buffer (Promega). Luciferase level was then analyzed by taking 20 µL of the cell lysate and 50 µL of luciferase reagent (Promega) in 500 µL tube and the sample was read in luminometer (Turner). The expression level of the treated samples was compared to the control samples.

2.6. RNA extraction and qPCR

Cells were lyzed in 350 µL Trizol Reagent (Sigma) and RNA extraction was performed using Direct-zol RNA miniprep kit (Zymogen) according to manufacturer's instructions. The quantity and quality of the RNA samples were analyzed with a DS-11 spectrophotometer (Denovix). cDNA synthesis was performed using qScript cDNA synthesis kit (Quanta Biosciences) with 500 µg of total RNA for each sample. Quantitative real-time PCR (qPCR) was carried out on a CFX96 Real-Time PCR Detection System (BioRad) using SsoAdvanced SYBR Green (BioRad) according to the manufacturer's instructions. Thermocycling conditions comprised a denaturation step at 95 ºC for 5 min, followed by 40 cycles at 95 ºC for 2 s and 60 ºC for 30 s. Gene expression levels were normalized using elongation factor (*E2F1*) and fold changes were calculated according to the ΔΔCt method (Schmittgen and Livak, 2008). The specific primers were obtained from previous study (Kharlyngdoh et al., 2018).

2.7. Statistical analysis

Statistical difference between treated and control groups was determined using One-way ANOVA followed by Dunnett's multiple comparisons test. Statistical analysis was performed using GraphPad Prism 8 software (GraphPad). Statistically significant differences were considered if the p values were < 0.05 (* $p < 0.05$, ** $p < 0.01$ and *** $p < 0.001$).

3. Results

3.1. Molecular modeling of hAR-ligand interactions

More than 90 crystal structures of the hAR-LBD with different ligands in all three binding sites have been previously reported (Sakkiah et al., 2016). However, no structure of the wild-type hAR-LBD with an antagonist in the LBP could be identified, presumably due to the experimental difficulties associated with the purification of these complexes (Bohl et al., 2005). For these types of antagonists as well as other molecules with no known binding poses, molecular modeling approaches involving molecular docking and dynamics simulations are frequently used (Duan et al., 2016; Jin et al., 2019; Liu et al., 2018; Prekovic et al., 2016; Sakkiah et al., 2018; Wahl and Smieško, 2018; Zhou et al., 2018). Here, we followed a similar procedure, and began with molecular docking simulations to generate hAR-LBD structures with bicalutamide, enzalutamide, linuron and procymidone (the structure of the hAR-LBD with dihydrotestosterone was already available from the Protein Data Bank, PDB code: 3L3X). Bicalutamide and enzalutamide are known to bind to the LBP of hAR, yet no prior information was available for procymidone and linuron.

Molecular docking simulations can be performed using a variety of programs. However, each program employs a specific search procedure and different scoring functions for pose generation and ranking. Moreover, they are validated using different sets of experimentally determined ligand-protein complexes. Here, we first performed a re-docking study to select a suitable molecular docking program for hAR-LBD ligands. For this purpose, we re-docked ligands into their respective binding sites (LBP, AF2, or BF3) in 19 experimental hAR-LBD structures (see Supplementary Table 1) using three academic molecular docking programs, LeDock (Liu and Xu, 2021), Autodock Vina (Trott and Olson, 2010), and GalaxyDock 3 (Yang et al., 2019).

According to our results, none of the molecular docking programs were able to successfully re-dock ligands onto AF2 and BF3 binding sites, as evidenced by Root Mean Square Distances (RMSD) to the experimental poses higher than 2 Å (Supplementary Fig. 2). For the LBP however, GalaxyDock 3 showed the best performance, as experimental poses of all ligands were correctly predicted by this program with high accuracy (at least one pose below 2 Å similarity was ranked among the top poses for each ligand) (Fig. 1). Based on these results, we excluded AF2 and BF3 sites from our analysis, and docked enzalutamide, bicalutamide, procymidone and linuron into hAR-LBD LBP (template structure taken from wt hAR – DHT complex, PDB code 3L3X) using GalaxyDock 3. Docking score was highest for DHT, followed by bicalutamide, enzalutamide, procymidone and linuron (Table 1).

3.2. Molecular dynamics (MD) simulations

Next, we conducted MD simulations using the complexes obtained from molecular docking simulations as starting conformations in order to assess structural changes in the hAR-LBD structure upon binding of different ligands. For bicalutamide-hAR-LBD, the simulation was further extended to 750 ns as equilibration was deemed incomplete after 500 ns. A ligand-free reference simulation was also conducted (after removing dihydrotestosterone). Since we used an agonist-bound hAR-LBD as receptor in docking simulations, we expected structural transitions in antagonist-bound complexes during MD simulations. Table 2 lists simulations conducted along with expected structural transitions.

RMSD time profiles of our simulations indeed indicate that DHT-hAR-LBD reached equilibrium earlier than all other complexes. This is expected, considering the direct use of the DHT-bound crystal structure in this simulation. For all other antagonists, we observed conformational changes until conformational equilibrium was reached at later time points. (Supplementary Fig. 3). Finally, we have also observed a highly fluctuating RMSD-time profile for ligand-free hAR-LBD, indicating the expected stabilization effect of ligand binding on hAR-LBD.

3.3. Contact patterns of ligands with hAR LBD in MD simulations

The difference between the docking scores of procymidone, linuron, DHT, bicalutamide and enzalutamide indicate different contact patterns with the hAR-LBD, which may determine whether a given ligand acts as an agonist or an antagonist. Thus, we next assessed the strength of interaction between each ligand with individual amino acid residues of

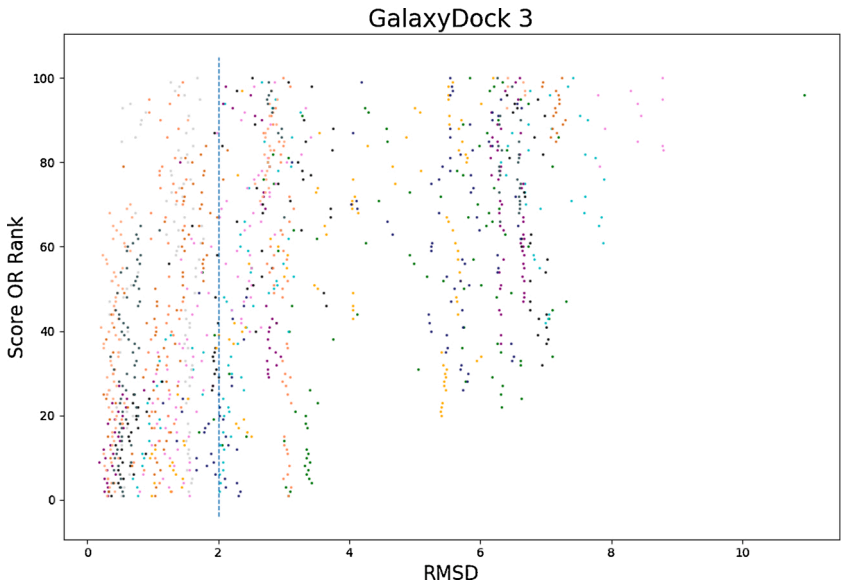

Fig. 1. Re-docking of hAR ligands into the hAR LBP using GalaxyDock 3. Each ligand listed in Supplementary Table 1 was re-docked into the hAR LBP using GalaxyDock 3. Different colors denote different ligands. Vertical dashed lines are drawn at 2 Å RMSD.

Table 1
GalaxyDock 3 docking scores for ligands included in this study.

Ligand	Score (kcal/mol)
Dihydrotestosterone	−92.50
Enzalutamide	−74.78
Bicalutamide	−85.20
Procymidone	−62.92
Linuron	−54.18

Table 2
Free energies of binding for ligands included in this study as predicted by PRODIGY-LIG.

Ligand	FEB (kcal/mol)
Dihydrotestosterone	−9.41 ± 0.16
Enzalutamide	−12.75 ± 0.25
Bicalutamide	−12.55 ± 0.37
Procymidone	−8.69 ± 0.13
Linuron	−7.53 ± 0.15

the hAR-LBD-LBP over the course of simulation trajectories. For this purpose, we used gRINN, which computes pairwise non-bonded force-field interaction energies between two pre-determined sets of residues. The results are plotted in the form of a heatmap in Fig. 2A.

Accordingly, the steroid DHT showed the highest interaction strength with N705, M787 and T877, in addition to several other residues including W741 and M895 of helix 12 (H12). Androgenic activity of the steroid scaffold is attributed to contacts with four critical hAR-LBD residues, namely N705, T877, Q711 and R752 (Tan et al., 2015). DHT maintained contact with two of these four amino acids (N705 and T877) in our MD simulations. Contact patterns of antagonists procymidone, linuron, bicalutamide and enzalutamide also indicated similar contacts with the hAR-LBD, with the exception of N705 contacts, which was only contacted by linuron. On the other hand, each antagonist made varying additional contacts with a stretch of LBP residues including M745, V746, M749, R752, F764, M780, N783 and C784, which did not interact with DHT. These residues are remarkably located away from the co-activator interaction site formed by H12 and portions of H3 and H4. Hence, contact made with these residues by hAR antagonist ligands may contribute to the overall antagonistic effect (Fig. 2B).

3.4. Per-residue mobilities in MD simulations

In order to assess the possible influence of the contact pattern differences given in the previous section on residue mobility, we next computed per-residue Root Mean Square Fluctuations (RMSF) profiles of hAR-LBD residues over the course of the simulation trajectory. The results are given in Fig. 3A. As expected, we observed the highest mobilities for the loop residues connecting the helices of the hAR LBD. The overall mobility profiles of different complexes were, however, mostly similar to each other. Here, two helices were affected by the ligand identity: H1 and H12. H12 apparently has a higher RMSF level with DHT than other ligands, expect for linuron. At other sites there are no clear differences between DHT and other ligands (except for H1 and loops). The bicalutamide RMSF profile was rather distinct from all other ligands in a few regions, as evidenced by clearly lower RMSF of H4 and the loop between H8 and H9. Also, the RMSF of H12 was lower than all other ligands as well.

3.5. Relative orientations of activation function 2 (AF2) helices

The AF2 co-activator binding site is formed by H12 and portions of H3 and H4. We thus inspected the relative orientations of these helices within simulation trajectories. For this purpose, we generated overlays of the AF2 site from a top-down angle using snapshots from each MD simulation trajectory (Fig. 3B). The orientations of AF2 helices with respect to each other were found to be different for each ligand/hAR-LBD pair, indicating that the AF2 site gets affected in different ways by each ligand. In order to quantify this effect, we computed pairwise distances over the course of simulations between the center-of-mass of each helix forming the AF2 site (Fig. 4). Here, DHT appeared to stabilize the interface as less fluctuation was observed in all the helices, expect for H4. Enzalutamide displaced H4, and also affected H12 slightly. Procymidone and linuron clearly caused rearrangement within H12. Procymidone also affected the orientation of H4 with respect to the other two helices. Moreover, procymidone decreased and increased H12-H3 and H12-H4 distances, respectively. Finally, bicalutamide surprisingly yielded a very stable binding interface, even rigidified all the helices. Nevertheless, this rigidification also caused a distinct increase in H3-H4 distance, indicating a clear disruption of the AF2 site upon bicalutamide binding.

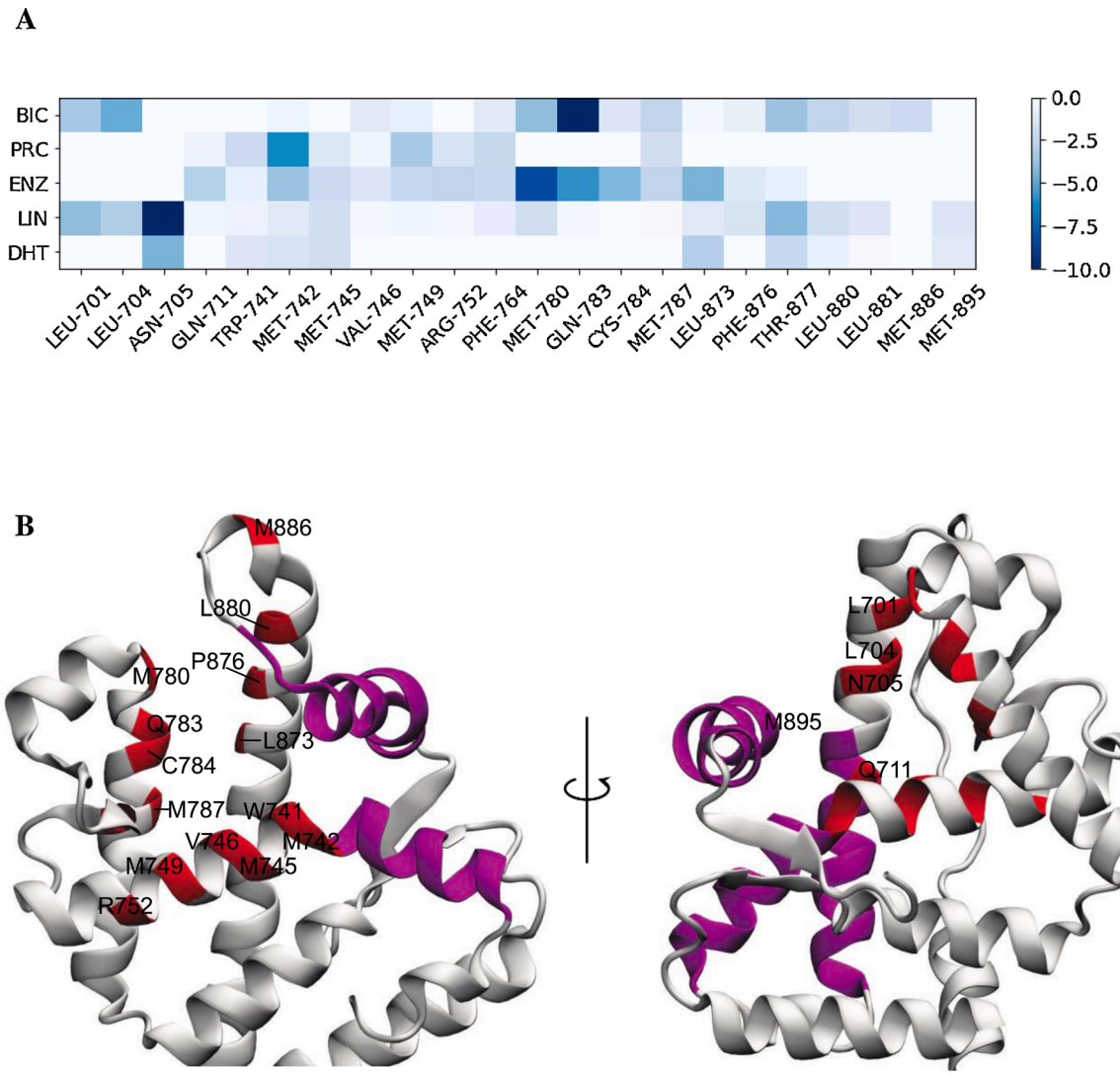

Fig. 2. hAR-LBD-ligand interaction energies. (A) Non-bonded interaction energies between each ligand and hAR-LBD-LBP residues are plotted in the form of a heatmap (units: kcal/mol) (A). Amino acid residues showing significant interaction with ligands (colored red) as determined from IE heatmap in (A) are distributed across AR-LBD helices. Residue groups forming the AF2 site are colored in magenta. Residue 669-722 and 840-890 are not shown for visual clarity in left and right views respectively (B).

3.6. Binding free energy (BFE) calculations

In addition to the effects on the hAR-LBD structure, binding free energies of different ligands also determine the affinity of each ligand to the hAR-LBD, and thereby the overall magnitude of their agonistic/antagonistic action. Here, we computed binding free energies of each ligand using PRODIGY-LIG method (Kurkcuoglu et al., 2018) on snapshots obtained from simulation trajectories. The results are given in Table 2. Accordingly, the highest average binding free energy was obtained for enzalutamide, followed by bicalutamide, DHT, procymidone, and linuron.

3.7. Procymidone and linuron show antiandrogenic activity in vitro

MDA-kb2 cell line stably expresses MMTV:luciferase which has androgen and glucocorticoid response element. Induction of this cell with androgens or glucocorticoids can result in increased luciferase activity. In order to determine EC_{50} of DHT, MDA-kb2 cells were exposed to different doses of DHT from 0.001–100 nM. EC_{50} was determined to be 0.18 nM (Fig. 5A) and from this EC85 (1 nM) was determined using GraphPad software. To analyze antiandrogenic activity, cells were exposed to procymidone and linuron in combination and alone with 1 nM of DHT. Exposure of cells only with procymidone and linuron did not show any luciferase activity which indicates that they do not have androgenic property (data not shown). However, both procymidone and linuron inhibited DHT mediated androgen activity (Fig. 5B). Linuron and procymidone were analyzed at 1 and 10 μM dose and their activity was compared to common AR inhibitors enzalutamide and bicalutamide. Linuron at 1 μM showed no activity while 10 μM dose resulted in 1.4-fold reduction of DHT mediated luciferase activation. On the other hand, procymidone at 1 μM and 10 μM showed 1.13- and 3.5-fold reduction respectively. The inhibition by procymidone at 10 μM was higher than inhibition observed by 1 and 10 μM of bicalutamide (2.5- and 2.8-fold reduction respectively) (Fig. 5B). The procymidone (10 μM) and enzalutamide (1 μM) mediated inhibition was equivalent.

Gene expression analysis following exposure of LNCaP cells showed that both procymidone and linuron downregulates androgen response genes including *prostate specific membrane antigen* (*PSA*) and *Microseminoprotein beta* (*MSMB*). As observed in luciferase assay, the 1 μM of linuron was not effective as it did not alter the expression of *PSA* and *MSMB* (Fig. 6A and B).

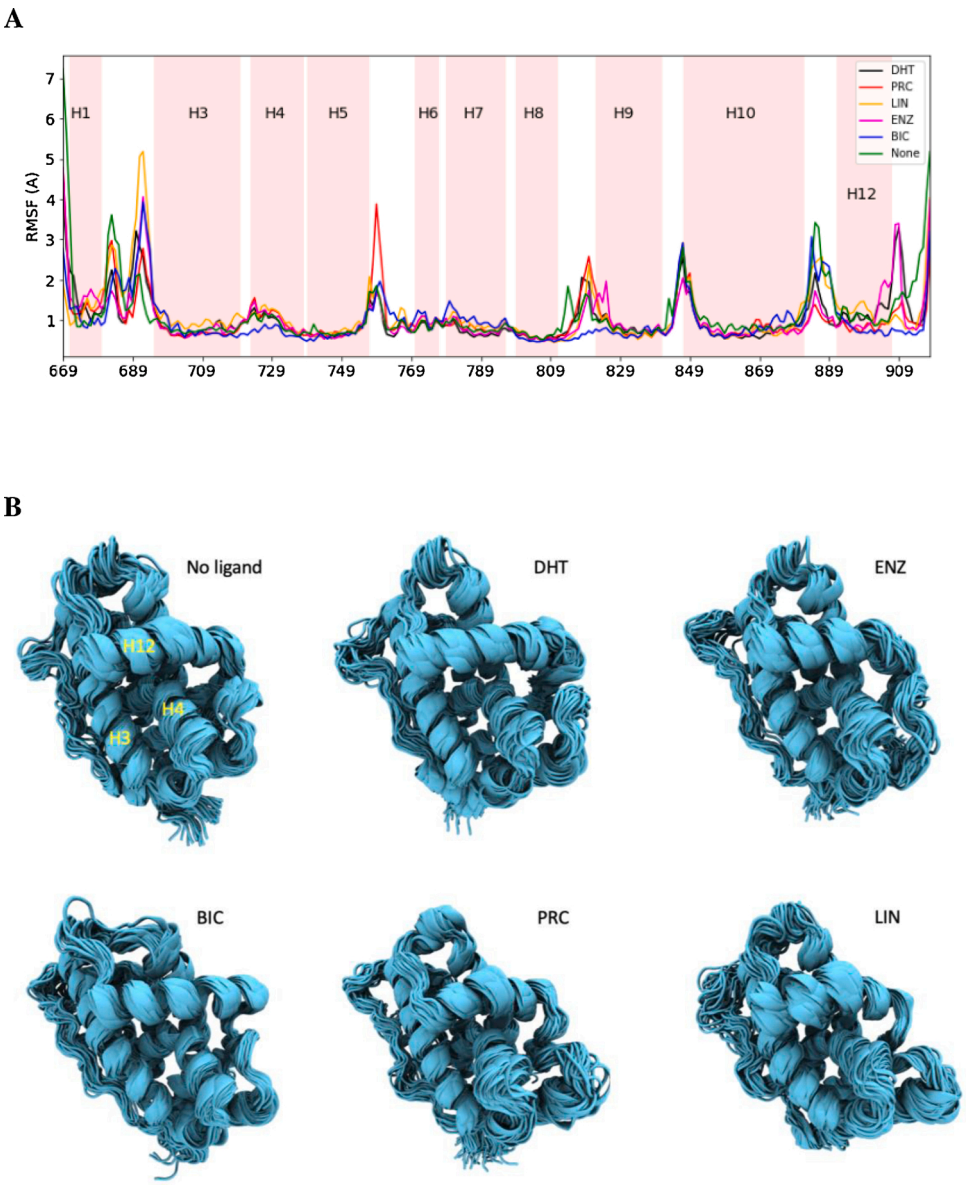

Fig. 3. Molecular flexibility and residue mobilities from molecular dynamics simulations. Per-residue Root mean square fluctuations (RMSF) indicate the overall mobility of individual amino acid residues during the molecular dynamics simulations (A). Overlay of snapshots from MD simulations. Ligands are omitted for visual clarity (B).

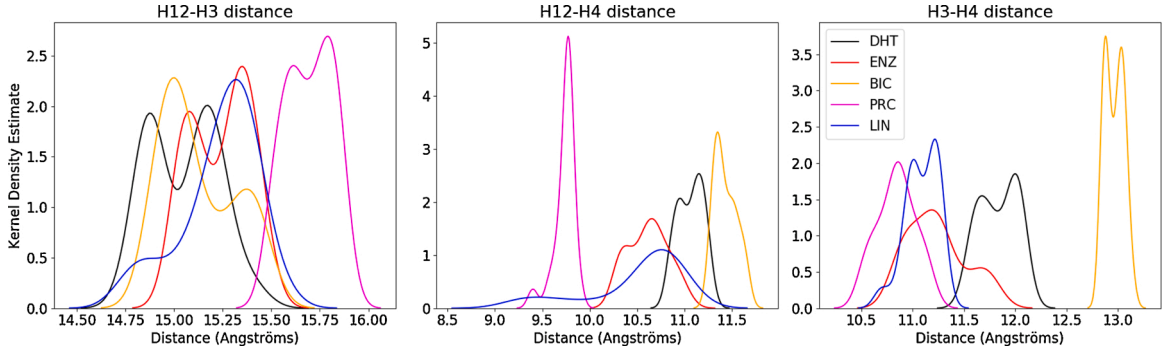

Fig. 4. Distributions of distances between helices forming the AF2 site (H12, H3 and H4) in MD simulations. Distances were calculated between the center of mass of each helix over the course of simulation trajectories.

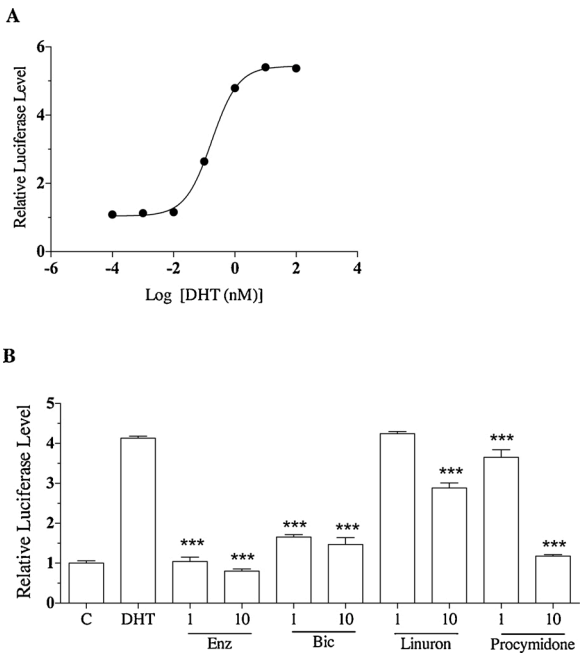

Fig. 5. AR antagonists inhibit luciferase activity. MDA-kb2 cells were treated with different concentrations of DHT to determine EC_{50} (A). MDA-kb2 cells were co-exposed with DHT and 1 and 10 μM of enzalutamide, bicalutamide, linuron and procymidone and luciferase levels were analyzed (B). One-way ANOVA followed by Dunnett's multiple comparisons test was performed. n = 4, (* $p < 0.05$, ** $p < 0.01$ and *** $p < 0.001$).

4. Discussion

Several studies have provided mechanistic insight into the agonist/antagonist action of hAR ligands using molecular modeling and MD simulations. Sakkiah et al. (Sakkiah et al., 2018) performed MD simulations to simulate structural changes upon the binding of bicalutamide to the hAR-LBD. They reported that some residues in the AF2 site are disrupted upon bicalutamide binding, and thereby caused a difference in electrostatic profiles. However, this disruption was not reflected in the overall per-residue mobility data reported in this study. In contrast, we observed an overall rigidification effect of bicalutamide on the AF2 site of hAR-LBD. In another study, Liu et al. (Liu et al., 2018) used MD simulations to probe allosteric communication between ligand binding pocket and AF2 site. They observed that DHT maintained native contacts (no structural changes) in contrast to antagonists. They also mapped connections between H4, H3, H12 and ligands, and demonstrated that co-activator binding is enhanced with agonists and weakens with antagonists. Jin et al. (Jin et al., 2019) focused on the same phenomenon, but with a different agonist/antagonist set. They reported conserved hydrogen bonds between DHT and N705 and T877. In this study, we also observed that these residues are critical for ligand-protein interaction. Apart from these two residues, A705, T741, M742, M745, M787 and F876 are also important. In our previous study using docking software Molecular Operating Environment, we showed that T877, N705, Q711 and R752 are important for ligand-AR interaction (Kharlyngdoh et al., 2015). The difference in residues involved in interaction could be due to the introduction of longer molecular dynamics in the present study.

The study by Singam et al., (Azhagiya Singam et al., 2019) compared structural dynamics of AR-LBD bound to several agonists and antagonists. Agonists included DHT, testosterone, R1881, and 17-beta-trenbolone, whereas antagonists were vinclozolin, neburon, bicalutamide, and hydroxyflutamide. They reported hydrogen bonds between bicalutamide and N705 and R752. In our simulations, we observed that bicalutamide interacted with L704, whereas the strongest interaction was with M780. These authors also found that only agonists formed

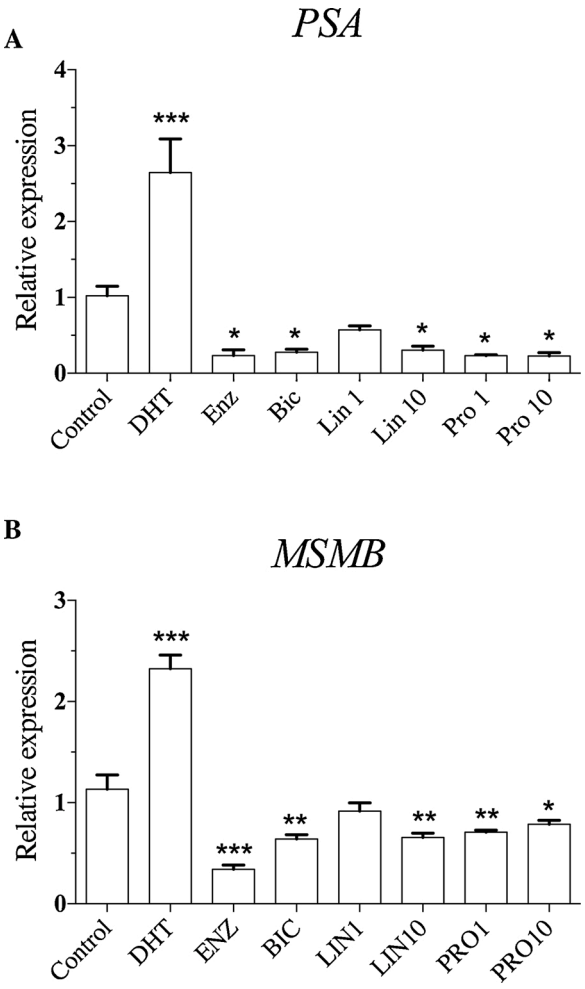

Fig. 6. AR antagonists downregulate AR response genes. LNCaP cells were exposed to 10 nM DHT, 10 μM of enzalutamide, 10 μM of bicalutamide and 1 and 10 yM of procymidone and linuron for 24 h and qRT-PCR was performed to determine the expression of *PSA* (A) and *MSMB* (B). One-way ANOVA followed by Dunnett's multiple comparisons test was performed. n = 4, (* $p < 0.05$, ** $p < 0.01$ and *** $p < 0.001$).

hydrogen bonds with N705 and T877. Liu et al. (Liu et al., 2017) investigated the molecular mechanism behind mutation-induced resistance of hAR-LBD to enzalutamide using MD simulations. Duan et al. (Duan et al., 2016) investigated structural differences between agonist- and antagonist-bound hAR-LBD in extensive MD simulations. Wu et al. (Wu et al., 2016) developed a classification methodology for discriminating antagonists from agonists from MD simulations. Finally, Galli et al. used molecular docking and low-mode MD simulations to investigate the androgenic affinity of several compounds with known endocrine activity including procymidone (Galli et al., 2014). A common finding in all these studies was the disruption of the H12 upon antagonist binding. In line with these observations, we also detected the highest effect of antagonist binding on H12. However, there was no clear pattern in terms of per-residue mobilities between the agonist DHT and antagonists linuron, procymidone, bicalutamide, and enzalutamide. Instead, we found differences between the contact patterns of DHT and antagonists linuron, procymidone, enzalutamide, and bicalutamide in MD simulations, which affected the relative orientations of helices that constitute the AF2 site. Another interesting finding from this study was the ranking of the hAR-LBD binding affinities of antagonists with respect to DHT in terms of binding free energies computed from MD simulations. Accordingly, enzalutamide showed the strongest affinity to hAR-LBD, followed by bicalutamide, DHT, procymidone and linuron in

decreasing order. Procymidone showed higher affinity to hAR compared to linuron and this could be attributed to the involvement of different residues in the AR-LBD. Procymidone and linuron showed a distinct interaction heat map. Interestingly, some of the interacting residues between procymidone and enzalutamide were the same.

To validate these findings, we performed *in vitro* studies on MDA-kb2 and LNCaP cells. Our results confirmed that procymidone and linuron have antagonistic activity to human AR. A comparison of potency and efficacy suggests that procymidone is a stronger antagonist than linuron. The study by Nellemann et al. (Nellemann et al., 2003) showed that procymidone can inhibit androgen mediated upregulation of luminescence *in vitro*. In the same study (Nellemann et al., 2003), CHO cells were co-exposed with procymidone and 0.01 nM of R1881 (an androgenic compound) and the IC_{50} for procymidone was determined to be 0.6 μM. In our study we have used 1 nM of DHT as EC85 concentration and we observed that procymidone at 10 μM shows similar inhibitory activity like enzalutamide at 1 μM. Our study and previous study confirm that procymidone has antagonistic activity. Procymidone is shown to decrease prostate weight in rats (Nellemann et al., 2003). Our study with prostate cell line LNCaP further shows that procymidone is detrimental to male reproductive health as it downregulated the *PSA* and *MSMB* genes which are important for the proper functioning of the prostate and commonly used as biomarkers for understanding prostate malfunction.

Linuron is a urea-based herbicide and it has been shown to have AR antagonistic activity. Using COS cell line, the binding activity of linuron against R1881 was found to be 20 μM and in reporter assay with 0.1 nM DHT, the IC50 was determined to be 10 μM (Lambright et al., 2000). In our study we observed that linuron at 1 μM does not have any effect in both reporter and gene expression analysis. Antagonistic effects were observed only at 10 μM dose. This further supports our claim that linuron is a weaker AR antagonist than procymidone. *In vivo* studies have also shown that procymidone is a stronger AR antagonist. Studies using castrated male rats showed that linuron significantly resulted in 38.4 % (Kang et al., 2004) and 33.0 % (Lambright et al., 2000), inhibition of testosterone propionate induced growth of the ventral prostate at 100 mg/kg per day, while procymidone at same dose showed 72.5 % (Kang et al., 2004) and 65.9 % (Nellemann et al., 2003) reduction in ventral prostate.

Taken together, our *in silico* and *in vitro* analysis is in line with the *in vivo* data. The results of our comparative *in vitro* analysis of inhibition strengths of procymidone and linuron with respect to well-known antagonists enzalutamide, bicalutamide also aligned well with our *in silico* binding affinity results. Furthermore, our *in silico* data provides valuable mechanistic insight into the differences between the inhibitory effects of these ligands at the molecular level.

5. Conclusion

In this study, we show that procymidone and linuron show distinct binding affinity to human AR and using *in vitro* analysis we further show that these compounds are AR antagonists. Many environmental pollutants that are released into the environment have been shown to modulate AR function. These pollutants can lead to reproductive and other physiological problems in animals and humans. Hence, it is important to analyze the chemicals for their endocrine disrupting effects. In the present study we have utilized both *in silico* and *in vitro* tools to show the molecular mechanisms of toxicity. Using this approach different endocrine disrupting chemicals should be screened which will help to reduce their use as well as introduce strict regulations on their production and usage.

Author statement

Conceptualization: AP and CB, OS
Experiments: AP, CB, OS
Data analysis: AP, CB, OS, PEO
Manuscript writing: AP, CB, OS
Manuscript editing: AP, CB, OS, PEO
Funding: PEO, AP

Declaration of Competing Interest

Authors declare that there is no conflict of interest.

Acknowledgement

This research was funded by Knowledge Foundation Sweden, O.E and Edla Johanssons Scientific Foundation, Sweden and Örebro University.

Appendix A. Supplementary data

Supplementary material related to this article can be found, in the online version, at doi:https://doi.org/10.1016/j.compbiolchem.2021.107490.

References

Azhagiya Singam, E.R., Tachachartvanich, P., La Merrill, M.A., Smith, M.T., Durkin, K.A., 2019. Structural dynamics of agonist and antagonist binding to the androgen receptor. J. Phys. Chem. B 123, 7657–7666.
Bai, J., Han, H., Wang, F., Su, L., Ding, H., Hu, X., Hu, B., Li, H., Zheng, W., Li, Y., 2017. Maternal linuron exposure alters testicular development in male offspring rats at the whole genome level. Toxicology 389, 13–20.
Bakan, A., Meireles, L.M., Bahar, I., 2011. ProDy: protein dynamics inferred from theory and experiments. Bioinformatics 27, 1575–1577.
Bohl, C.E., Gao, W., Miller, D.D., Bell, C.E., Dalton, J.T., 2005. Structural basis for antagonism and resistance of bicalutamide in prostate cancer. Proc Natl Acad Sci U S A 102, 6201–6206.
Dabrowski, J., Peall, S., Reinecke, A., Liess, M., Schulz, R., 2002. Runoff-related pesticide input into the Lourens River, South Africa: basic data for exposure assessment and risk mitigation at the catchment scale. Water Air Soil Pollut. 135, 265–283.
Davey, R.A., Grossmann, M., 2016. Androgen receptor structure, function and biology: from bench to bedside. Clin. Biochem. Rev. 37, 3–15.
Duan, M., Liu, N., Zhou, W., Li, D., Yang, M., Hou, T., 2016. Structural diversity of ligand-binding androgen receptors revealed by microsecond long molecular dynamics simulations and enhanced sampling. J. Chem. Theory Comput. 12, 4611–4619.
Earl Gray Jr., L., Wilson, V.S., Stoker, T., Lambright, C., Furr, J., Noriega, N., Howdeshell, K., Ankley, G.T., Guillette, L., 2006. Adverse effects of environmental antiandrogens and androgens on reproductive development in mammals 1. Int. J. Androl. 29, 96–104.
EPA, U, 2015. EDSP: Weight of Evidence Analysis of Potential Interaction With the Estrogen, Androgen or Thyroid Pathways. Chemical: Glyphosate. Office of Pesticide Programs US EPA, Washington DC, USA.
Foster, P.M., 2006. Disruption of reproductive development in male rat offspring following in utero exposure to phthalate esters. Int. J. Androl. 29, 140–147.
Freires, I.A., Sardi, Jd.C.O., de Castro, R.D., Rosalen, P.L., 2017. Alternative animal and non-animal models for drug discovery and development: bonus or burden? Pharma Res 34, 681–686.
Freyberger, A., Schladt, L., 2009. Evaluation of the rodent Hershberger bioassay on intact juvenile males–testing of coded chemicals and supplementary biochemical investigations. Toxicology 262, 114–120.
Freyberger, A., Weimer, M., Tran, H.S., Ahr, H.J., 2010. Assessment of a recombinant androgen receptor binding assay: initial steps towards validation. Reprod. Toxicol. 30, 2–8.
Galli, C.L., Sensi, C., Fumagalli, A., Parravicini, C., Marinovich, M., Eberini, I., 2014. A computational approach to evaluate the androgenic affinity of iprodione, procymidone, vinclozolin and their metabolites. PLoS One 9.
Hollingsworth, S.A., Dror, R.O., 2018. Molecular dynamics simulation for all. Neuron 99, 1129–1143.
Hosokawa, S., Murakami, M., Ineyama, M., Yamada, T., Yoshitake, A., Yamada, H., Miyamoto, J., 1993. The affinity of procymidone to androgen receptor in rats and mice. J. Toxicol. Sci. 18, 83–93.
Hospital, A., Goñi, J.R., Orozco, M., Gelpí, J.L., 2015. Molecular dynamics simulations: advances and applications. Adv. Appl. Bioinformatics Chem. Adv Appl Bioinform Chem 8, 37.
Hotchkiss, A., Parks-Saldutti, L., Ostby, J., Lambright, C., Furr, J., Vandenbergh, J., Gray Jr., L., 2004. A mixture of the "antiandrogens" linuron and butyl benzyl phthalate alters sexual differentiation of the male rat in a cumulative fashion. Biol. Reprod. 71, 1852–1861.
Jin, Y., Duan, M.J., Wang, X.W., Kong, X.T., Zhou, W.F., Sun, H.Y., Liu, H., Li, D., Yu, H. D., Li, Y.Y., Hou, T.J., 2019. Communication between the ligand-binding pocket and the activation Function-2 domain of androgen receptor revealed by molecular dynamics simulations. J. Chem. Inf. Model. 59, 842–857.

Jurado, A., Fernandes, M., Videira, R., Peixoto, F., Vicente, J., 2011. Herbicides: the face and the reverse of the coin. An in vitro approach to the toxicity of herbicides in non-target organisms. Herbicides Environ 1–44.
Kang, I.H., Kim, H.S., Shin, J.H., Kim, T.S., Moon, H.J., Kim, I.Y., Choi, K.S., Kil, K.S., Park, Y.I., Dong, M.S., Han, S.Y., 2004. Comparison of anti-androgenic activity of flutamide, vinclozolin, procymidone, linuron, and p, p'-DDE in rodent 10-day Hershberger assay. Toxicology 199, 145–159.
Kharlyngdoh, J.B., Pradhan, A., Asnake, S., Walstad, A., Ivarsson, P., Olsson, P.E., 2015. Identification of a group of brominated flame retardants as novel androgen receptor antagonists and potential neuronal and endocrine disrupters. Environ. Int. 74, 60–70.
Kharlyngdoh, J.B., Pradhan, A., Olsson, P.E., 2018. Androgen receptor modulation following combination exposure to brominated flame-retardants. Sci. Rep. 8, 4843.
Kojima, H., Katsura, E., Takeuchi, S., Niiyama, K., Kobayashi, K., 2004. Screening for estrogen and androgen receptor activities in 200 pesticides by in vitro reporter gene assays using Chinese hamster ovary cells. Environ. Health Perspect. 112, 524–531.
Kortenkamp, A., Faust, M., 2010. Combined exposures to anti-androgenic chemicals: steps towards cumulative risk assessment. Int. J. Androl. 33, 463–474.
Kunzmann, P., Hamacher, K., 2018. Biotite: a unifying open source computational biology framework in Python. BMC Bioinformatics 19, 346.
Kurkcuoglu, Z., Koukos, P.I., Citro, N., Trellet, M.E., Rodrigues, J.P.G.L.M., Moreira, I.S., Roel-Touris, J., Melquiond, A.S.J., Geng, C.L., Schaarschmidt, J., Xue, L.C., Vangone, A., Bonvin, A.M.J.J., 2018. Performance of HADDOCK and a simple contact-based protein-ligand binding affinity predictor in the D3R Grand Challenge 2. J Comput Aided Mol Design 32, 175–185.
Lambright, C., Ostby, J., Bobseine, K., Wilson, V., Hotchkiss, A., Mann, P., Gray Jr., L., 2000. Cellular and molecular mechanisms of action of linuron: an antiandrogenic herbicide that produces reproductive malformations in male rats. Toxicol. Sci. 56, 389–399.
Liu, N., Xu, Z., 2021. Using LeDock As a Docking Tool for Computational Drug Design, 1 ed. IOP Publishing. pp. 012143-012143.
Liu, H., Wang, L., Tian, J., Li, J., Liu, H., 2017. Molecular dynamics studies on the enzalutamide resistance mechanisms induced by androgen receptor mutations. J. Cell. Biochem. 118, 2792–2801.
Liu, N., Zhou, W.F., Guo, Y., Wang, J.M., Fu, W.T., Sun, H.Y., Liu, D., Duan, M.J., Hou, T. J., 2018. Molecular dynamics simulations revealed the regulation of ligands to the interactions between androgen receptor and its coactivator. J. Chem. Inf. Model. 58, 1652–1661.
Malde, A.K., Zuo, L., Breeze, M., Stroet, M., Poger, D., Nair, P.C., Oostenbrink, C., Mark, A.E., 2011. An automated force field topology builder (ATB) and repository: version 1.0. J. Chem. Theory Comput. 7, 4026–4037.
Marker, P.C., Donjacour, A.A., Dahiya, R., Cunha, G.R., 2003. Hormonal, cellular, and molecular control of prostatic development. Dev. Biol. (Basel) 253, 165–174.
Nellemann, C., Dalgaard, M., Lam, H.R., Vinggaard, A.M., 2003. The combined effects of vinclozolin and procymidone do not deviate from expected additivity in vitro and in vivo. Toxicol. Sci. 71, 251–262.
Oliver, D.P., Kookana, R.S., Anderson, J.S., Cox, J.W., Fleming, N., Waller, N., Smith, L., 2012. Off-site transport of pesticides from two horticultural land uses in the Mt. Lofty Ranges, South Australia. Agric. Water Manag. 106, 60–69.
Orton, F., Lutz, I., Kloas, W., Routledge, E.J., 2009. Endocrine disrupting effects of herbicides and pentachlorophenol: in vitro and in vivo evidence. Environ. Sci. Technol. 43, 2144–2150.
Ostby, J., Kelce, W.R., Lambright, C., Wolf, C.J., Mann, P., Gray Jr., L.E., 1999. The fungicide procymidone alters sexual differentiation in the male rat by acting as an androgen-receptor antagonist in vivo and in vitro. Toxicol. Ind. Health 15, 80–93.
Prekovic, S., Van Royen, M.E., Voet, A.R.D., Geverts, B., Houtman, R., Melchers, D., Zhang, K.Y.J., Van Den Broeck, T., Smeets, E., Spans, L., Houtsmuller, A.B., Joniau, S., Claessens, F., Helsen, C., 2016. The effect of F877L and T878A mutations on androgen receptor response to enzalutamide. Mol Cancer Therap 15, 1702–1712.
Quintaneiro, C., Patrício, D., Novais, S., Soares, A., Monteiro, M., 2017. Endocrine and physiological effects of linuron and S-metolachlor in zebrafish developing embryos. Sci. Total Environ. 586, 390–400.
Radice, S., Fumagalli, R., Chiesara, E., Ferraris, M., Frigerio, S., Marabini, L., 2004. Estrogenic activity of procymidone in rainbow trout (Oncorhynchus mykiss) hepatocytes: a possible mechanism of action. Chemico Biol Int 147, 185–193.
Radice, S., Chiesara, E., Frigerio, S., Fumagalli, R., Parolaro, D., Rubino, T., Marabini, L., 2006. Estrogenic effect of procymidone through activation of MAPK in MCF-7 breast carcinoma cell line. Life Sci. 78, 2716–2723.
Sakkiah, S., Ng, H.W., Tong, W., Hong, H., 2016. Structures of Androgen Receptor Bound With Ligands: Advancing Understanding of Biological Functions and Drug Discovery, pp. 1267–1282.
Sakkiah, S., Kusko, R., Pan, B.H., Guo, W.J., Ge, W.G., Tong, W.D., Hong, H.X., 2018. Structural changes due to antagonist binding in ligand binding pocket of androgen receptor elucidated through molecular dynamics simulations. Front. Pharmacol. 9.
Schmittgen, T.D., Livak, K.J., 2008. Analyzing real-time PCR data by the comparative C_T method. Nat. Protoc. 3, 1101–1108.
Schuler, L.J., Rand, G.M., 2008. Aquatic risk assessment of herbicides in freshwater ecosystems of south Florida. Arch. Environ. Contam. Toxicol. 54, 571–583.
Sercinoglu, O., Ozbek, P., 2018. gRINN: a tool for calculation of residue interaction energies and protein energy network analysis of molecular dynamics simulations. Nucleic Acids Res. 46, W554–W562.
Spirhanzlova, P., De Groef, B., Nicholson, F.E., Grommen, S.V., Marras, G., Sébillot, A., Demeneix, B.A., Pallud-Mothré, S., Lemkine, G.F., Tindall, A.J., 2017. Using short-term bioassays to evaluate the endocrine disrupting capacity of the pesticides linuron and fenoxycarb. Comp. Biochem. Physiol. C Toxicol. Pharmacol. 200, 52–58.
Tan, M.H., Li, J., Xu, H.E., Melcher, K., Yong, E.L., 2015. Androgen receptor: structure, role in prostate cancer and drug discovery. Acta Pharmacol. Sin. 36, 3–23.
Tomigahara, Y., Suzuki, N., Tarui, H., Saito, K., Kaneko, H., 2014. Anti-androgenic activity of procymidone and its metabolites. J Pesticide Sci D14–059.
Trott, O., Olson, A.J., 2010. Software news and update AutoDock Vina: improving the speed and accuracy of docking with a new scoring function, efficient optimization, and multithreading. J. Comput. Chem. 31, 455–461.
Uren Webster, T.M., Perry, M.H., Santos, E.M., 2015. The herbicide linuron inhibits cholesterol biosynthesis and induces cellular stress responses in brown trout. Environ. Sci. Technol. 49, 3110–3118.
Vinggaard, A.M., Joergensen, E.C.B., Larsen, J.C., 1999. Rapid and sensitive reporter gene assays for detection of antiandrogenic and estrogenic effects of environmental chemicals. Toxicol. Appl. Pharmacol. 155, 150–160.
Vinggaard, A.M., Niemela, J., Wedebye, E.B., Jensen, G.E., 2008. Screening of 397 chemicals and development of a quantitative structure–activity relationship model for androgen receptor antagonism. Chem. Res. Toxicol. 21, 813–823.
Wahl, J., Smieško, M., 2018. Endocrine disruption at the androgen receptor: employing molecular dynamics and docking for improved virtual screening and toxicity prediction. Int. J. Mol. Sci. 19, 1784-1784.
Wang, X.-D., Wang, B.-E., Soriano, R., Zha, J., Zhang, Z., Modrusan, Z., Cunha, G.R., Gao, W.-Q., 2007. Expression profiling of the mouse prostate after castration and hormone replacement: implication of H-cadherin in prostate tumorigenesis. Differentiation 75, 219–234.
Wilson, V.S., Cardon, M.C., Gray Jr., L.E., Hartig, P.C., 2007. Competitive binding comparison of endocrine-disrupting compounds to recombinant androgen receptor from fathead minnow, rainbow trout, and human. Environ. Toxicol. Chem. 26, 1793–1802.
Wilson, V.S., Blystone, C.R., Hotchkiss, A.K., Rider, C.V., Gray Jr., L.E., 2008. Diverse mechanisms of anti-androgen action: impact on male rat reproductive tract development. Int. J. Androl. 31, 178–187.
Wilson, V.S., Lambright, C.R., Furr, J.R., Howdeshell, K.L., Gray Jr., L.E., 2009. The herbicide linuron reduces testosterone production from the fetal rat testis during both in utero and in vitro exposures. Toxicol. Lett. 186, 73–77.
Woudneh, M.B., Ou, Z., Sekela, M., Tuominen, T., Gledhill, M., 2009. Pesticide multiresidues in waters of the lower Fraser valley, British Columbia. Canada. Part I. Surface water. J Environ Quality 38, 940–947.
Wu, Y., Doering, J.A., Ma, Z., Tang, S., Liu, H., Zhang, X., Wang, X., Yu, H., 2016. Identification of androgen receptor antagonists: in vitro investigation and classification methodology for flavonoid. Chemosphere 158, 72–79.
Wu, Y., Zuo, Z., Chen, M., Zhou, Y., Yang, Q., Zhuang, S., Wang, C., 2018. The developmental effects of low-level procymidone towards zebrafish embryos and involved mechanism. Chemosphere 193, 928–935.
Yang, J., Baek, M., Seok, C., 2019. GalaxyDock3: protein–ligand docking that considers the full ligand conformational flexibility. J. Comput. Chem. 40, 2739–2748.
Zheng, S., Chen, B., Qiu, X., Chen, M., Ma, Z., Yu, X., 2016. Distribution and risk assessment of 82 pesticides in Jiulong River and estuary in South China. Chemosphere 144, 1177–1192.
Zhou, W., Duan, M., Fu, W., Pang, J., Tang, Q., Sun, H., Xu, L., Chang, S., Li, D., Hou, T., 2018. Discovery of novel androgen receptor ligands by structure-based virtual screening and bioassays. Genomics Proteomics Bioinformatics 16, 416–427.